# Processing Seismic Ambient Noise Data with the Continuous Wavelet Transform to Obtain Reliable Empirical Green's Functions

Yang Yang[1]

Chunyu Liu[1]

Charles A. Langston[1]

[1]Center for Earthquake Research and Information
University of Memphis
3876 Central Ave., Suite 1
Memphis, TN 38152

Submitted to the
*Geophysical Journal International*
on August 17, 2019

Running title: Processing Seismic Ambient Noise Data with the CWT

Yang.Yang@memphis.edu
cliu5@memphis.edu
clangstn@memphis.edu

## SUMMARY

We propose a new data processing flow to compute empirical Green's functions (EGF) from ambient seismic noise based on a soft thresholding designaling and denoising method using the continuous wavelet transform. The designaling algorithm is carried out during the initial data processing to remove earthquakes and other transient signals in the seismic record. A continuous wavelet transform denoising algorithm removes the noise in the final stacked cross-correlogram. The overall data processing procedure is divided into four stages: (1) single station data preparation, (2) remove earthquakes and other signals in the seismic record, (3) spectrum whitening, cross-correlation and temporal stacking, (4) remove the noise in the stacked cross-correlogram to deliver the final EGF. The whole process is automated to make it accessible for large datasets. Synthetic data constructed with a recorded earthquake and recorded ambient noise is used to test the designaling method. We then apply the new processing flow to data recorded by the USArray Transportable Array stations near the New Madrid Seismic Zone where many seismic events and transient signals are observed in the data. We compare the EGFs calculated from our new flow with time domain normalization and our results show improved signal-to-noise ratios and deliver more reliable measurements that can be used for further processing. The designaling method improves the homogeneity of the ambient noise wavefield which is an intrinsic requirement for seismic interferometry. The final denoising step suppresses random noise and provides clearer EGFs for the next processing step.

Keywords: Seismic interferometry, seismic noise, wavelet transform

## INTRODUCTION

Cross-correlation of diffuse wave fields, such as from ambient noise or scattered coda waves, can be used to estimate the medium Green's function termed the empirical Green's function (EGF) between a pair of stations (e.g. Shapiro et al. 2005; Sabra et al. 2005; Wapenaar & Fokkema 2006). This method has been widely applied to data collected in different regions over the past 15 years to extract surface waves and body waves. Densely deployed networks have provided an opportunity for high-resolution surface wave tomography (e.g. Yao et al. 2006; Lin et al. 2008; Bensen et al. 2008) and full waveform inversion (e.g. Gao & Shen 2014; Emry et al. 2018). In spite of these applications, there have been fewer efforts to develop improved ambient noise data processing procedures in order to acquire more reliable and higher signal-to-noise ratio (SNR) EGFs. Bensen et al. (2007) summarized and compared different procedures on the use of seismic records to obtain surface wave dispersion measurements and their suggestions are still the main procedures that are generally used today to process ambient noise data.

Ground motion produced by earthquakes and other sources, such as non-stationary noise sources near a station or weather storm signals, will be recorded on the seismogram and are often considered as "useful signals" that contain important information about the seismic source and underground structure. However, in ambient noise tomography, these signals destroy the diffuse wave field assumption and need to be considered as "noise" in correlation processing. One of the most important steps during the processing is to remove these signals to obtain as "pure" ambient noise as possible. In Bensen et al. (2007), this step is called "time-domain normalization" or "temporal normalization", which is a procedure for reducing the effect of earthquakes, instrumental irregularities and non-stationary noise sources near to stations on the cross-correlations. This process balances the amplitude of ambient noise relative to the amplitude of

unwanted signals. Here, "signal" and "noise" are related to what is being studied and depend on whether removing "signal" or "noise" is useful for our purpose. Earthquakes and other source "signals" should be removed before cross-correlation because large amplitude signals at zero-delay time in the cross-correlation disguise the surface wave arrival from the microseisms. To avoid confusion, based on the common way of naming "ambient noise", we call the removing of earthquakes and other non-stationary noise source "signals" as designaling in this paper although the mathematics of doing so is the same as denoising.

Bensen et al. (2007) summarized different methods for identifying and removing earthquakes and other contaminants from the original recordings. These include 1-bit normalization, running absolute mean normalization and water level normalization that all suppress the contaminating signals. However, amplitude information is not fully retained in the cross-correlation because of the inherent amplitude down-weighting process in these methods. Amplitude is of fundamental importance for body wave anelastic attenuation estimation and basement resonance estimation based on the horizontal to vertical amplitude ratio (H/V ratio) of surface waves. Bensen et al. (2007) also suggested using running absolute mean normalization as the best practice to process the ambient noise data. In the rest of this paper, we will call this method as "time domain normalization" and it will be used as the benchmark method for comparison.

Removing transient signals while not touching the ambient noise itself is a crucial requirement for successful ambient noise data processing. We propose a method based on the Continuous Wavelet Transform (CWT) for dealing with this problem. The CWT has been widely used to for seismic analysis and denoising purposes (Pazos et al. 2003; Chik et al. 2009; To et al. 2009; Ansari et al. 2010; Beenamol et al. 2012; Mousavi & Langston 2016; Mousavi et al. 2016).

Compared with other denoising methods, using the CWT to achieve denoising has many natural translation-invariant and time-frequency properties such as reducing pseudo-Gibbs artifacts in the denoised signal (Elad & Aharon, 2006). In ambient noise data, the noise record usually dominates the time series with earthquakes or other transient signals contaminating only a small portion of the whole record. The statistical properties of the ambient noise can be estimated based on a segment of the noise record and time-frequency CWT analysis allows us to navigate the rest of data and remove the unwanted signals. The CWT provides one of the best choices for ambient noise designaling. Unlike its normal purpose for removing noise, we use this method in a reverse manner to take the signal out and keep the background ambient noise.

The motivation of this paper is to introduce a designaling procedure based on the CWT and apply it to ambient noise data processing. We also use essentially the same method to remove noise in the final stacked cross-correlograms. Details of the designaling and denoising methods will be given and then explored using a synthetic data example. Next, we use our new ambient noise processing flow to process data collected from EarthScope's USArray Transportable Array within the northern Mississippi embayment. The New Madrid Seismic Zone (NMSZ) inside of the Mississippi embayment is one of the most earthquake-active intraplate regions in North America (Hildenbrand, 1985; Cox et al., 2001; Tuttle et al., 2002; Thomas, 2006; Van Arsdale et al., 2007; Powell et al., 2010; Dunn et al., 2013; Van Arsdale and Cupples, 2013; Nyamwandha et al., 2016; Yang & Langston, 2019). Abundance of seismic events in the NMSZ could be used to test the efficiency and robustness of our method. Using the real data, the resulting EGFs and the final dispersion curves obtained from our method and Bensen's method are compared.

## CWT DENOISING AND DESIGNALING

### CWT

The CWT (Daubechies 1992) is a popular tool to study time-frequency representations of continuous or discrete time series. This mathematical transformation decomposes a signal into different scales as a function of time. Different scales provide different resolutions (or can be considered as different pseudo-frequency components) of the original signal. From this point of view, it provides better resolution compared to the short time Fourier transform (Tary et al. 2014). Assuming we have a time series $s(t)$, for a given mother wavelet $\psi(t)$, the CWT of time series $s(t)$ at scale $a$ ($a > 0$) and time shift $b$ can be expressed as (Daubechies 1992)

$$Ws(a,b) = \int_{-\infty}^{+\infty} s(t) a^{-1/2} \psi^* \left(\frac{t-b}{a}\right) dt, \tag{1}$$

where the $*$ indicates the complex conjugate and $Ws(a,b)$ is the wavelet coefficient representation of the signal $s(t)$ at scale $a$ and time shift $b$. The Fourier transform of the mother wavelet $\psi(t)$ should satisfy the admissibility condition (Daubechies 1992; Farge 1992)

$$0 < C_\psi = \int_{-\infty}^{+\infty} |\omega|^{-1} \left|\hat{\psi}(\omega)\right|^2 d\omega < \infty, \tag{2}$$

in which $\widehat{\psi}(\omega)$ is the Fourier transform of the mother wavelet $\psi(t)$ and $C_\psi$ is called the wavelet admissibility constant. Such a wavelet is called an admissible wavelet. An admissible wavelet also implies that $\hat{\psi}(0) = 0$ so that the integration over time must be zero (Daubechies 1992). To recover the original signal from the CWT representations, the inverse CWT can be expressed as

$$s(t) = \frac{1}{C_\psi} \int_0^\infty \int_{-\infty}^{+\infty} \frac{1}{\sqrt{a}} Ws(a,b)\, \psi \left(\frac{t-b}{a}\right) \frac{dadb}{a^2}. \tag{3}$$

The CWT of a discrete time series can be expressed in the similar way by replacing integration with summation (Torrence & Compo 1998) and different fast algorithms are

developed to make it computation affordable (Rioul & Duhamel 1992). In another mathematical view of equation (1), the CWT can be considered as a cross-correlation of the target time series $s(t)$ with different wavelets that are stretched or compressed and shifted versions of the selected mother wavelet $\psi(t)$. Because of this cross-correlation property, the CWT can be calculated using the fast Fourier transform (FFT) in the frequency domain (Daubechies 1992). The CWT spectrum $Ws(a,b)$ for the time series $s(t)$ is the time-frequency decomposition of the original signal, with different scales $a$ analogous to wave period (inverse frequency) and $b$ indicating time lag.

**Designaling and denoising via soft thresholding**

Langston & Mousavi (2019) discussed an efficient method based on the CWT to denoise or designal a time series using the statistical estimation of the noise. In this study, we implement the soft thresholding method in the ambient noise data processing flow. Essentially, the noise is estimated and then removed for different scales of wavelets by a less severe manner. The size of datasets used for ambient noise tomography is usually very large. Thus, processing ambient noise data requires an algorithm that is not time-consuming and works efficiently. Soft thresholding (Weaver et al., 1991) can remove noise efficiently compared to computationally intensive block thresholding algorithms on the wavelet scale-time plane (Mousavi & Langston, 2016).

In order to apply the CWT soft thresholding denoising, the original time series $s(t)$ is first transformed into the CWT time-frequency domain to get the CWT spectrum $Ws(a,b)$. The noise level for a specific scale $a$ is estimated and the CWT coefficients for this scale are modified by the non-linear soft thresholding given by

$$\bar{W}s(a,b) = \begin{cases} sign[Ws(a,b)](\|Ws(a,b)\| - \beta(a)) \; if \; \|Ws(a,b)\| \geq \beta(a) \\ 0 \qquad\qquad otherwise \end{cases}, \tag{4}$$

where

$$sign[Ws(a,b)] = \frac{Ws(a,b)}{\|Ws(a,b)\|}, \tag{5}$$

$\bar{W}s(a,b)$ is the CWT spectrum after denoising for the scale $a$ and $\|\cdot\|$ stands for the modulus of the complex spectrum in the CWT domain. The threshold function $\beta(a)$ is determined based on the statistics of the absolute value of the noise for scale $a$. If the CWT spectrum is less than $\beta(a)$, it is considered as the noise and we will remove it by setting it to zero. Otherwise, it contains both noise and signal, and the predefined noise is subtracted from the original spectrum. This criterion is applied to data at each scale in the CWT spectrum. Ambient noise data is continuously recorded and earthquakes and other signals only make up a small proportion of the whole record. The noise level $\beta(a)$ can be well estimated with a predetermined time segment which contains only ambient noise. Much of the signal processing procedures start from an assumption of Gaussian noise. The threshold function can be computed using the mean and standard deviation of the CWT spectrum for scale $a$ within the selected time segment:

$$\beta(a) = mean(\|Ws(a,b)\|) + N \; std(\|Ws(a,b)\|), \tag{6}$$

where

$$mean(\|Ws(a,b)\|) = \frac{1}{T_2 - T_1}\int_{T1}^{T2} \|Ws(a,b)\| \, db, \tag{7}$$

$$std(\|Ws(a,b)\|) = [\frac{1}{T_2 - T_1}\int_{T1}^{T2} (\|Ws(a,b)\| - mean(\|Ws(a,b)\|))^2 \, db]^{\frac{1}{2}}, \tag{8}$$

and $N$ is a parameter that controls the threshold noise level. The time limits $T_1$ and $T_2$ represent the start and end time of the selected time segment.

There are different criteria to choose the threshold coefficient, $N$, in equation (6). Simply choosing $N = 3$ will yield a signal at 99.7% confidence level (Starck et al., 2010) if the CWT coefficients of the noise follow a normal distribution. This method is straightforward to estimate the noise level. But unfortunately, the assumption that the CWT coefficients follow a Gaussian distribution is rarely seen in seismic noise data (Langston & Mousavi, 2019). The distribution for real ambient noise is usually unpredictable. However, we can estimate a data-driven noise level by taking the approach of empirically estimating the cumulative distribution of noise and then calculating the 99% confidence value for the distribution. To calculate the empirical cumulative distribution function (ECDF), we can order the N samples noise values and then assign a probability jump of 1/N when a value is attained, starting with the smallest value. Thus, the threshold function becomes:

$$\beta(a) = \mathrm{ECDF}^{-1}(P = 0.99), \tag{9}$$

where $\mathrm{ECDF}^{-1}$ is the inverse of the cumulative distribution function or the quantile.

In Fig. 1, we compare the threshold functions assuming Gaussian statistics in equation (6) and non-Gaussian statistics in equation (9). The distribution of the empirical probability distribution function of the real noise is different compared to a Gaussian distribution and gives quite different estimated noise levels. Overall, there are significant differences between the ECDF and Gaussian threshold functions. It also suggests that the ECDF method would lead to a better estimate of the threshold and thus we use the ECDF method to estimate the noise level in our processing. Fig.1

Designaling reverses the denoising process. This procedure can be applied in our ambient noise processing to remove earthquakes and other signals. For the soft thresholding case, signal is removed by using

$$\bar{W}s(a,b) = \begin{cases} sign[Ws(a,b)]\beta(a) \; if \; \|Ws(a,b)\| \geq \beta(a) \\ Ws(a,b) \qquad\qquad otherwise \end{cases}. \tag{10}$$

193 At each scale, if the CWT spectrum is less than the estimated noise level, we consider it as the
194 noise and keep the spectrum. Otherwise, we consider it as the signal and remove it by setting the
195 coefficient to the noise level.

196 Using the soft thresholding method to remove noise or signal based on ECDF is very
197 straightforward and efficient. After applying equation (4) for denoising or equation (10) for
198 designaling, we get our new CWT spectrum and get the final denoised or designaled output for
199 our next processing step by doing the inverse CWT from equation (3).

200

201 **DATA AND DATA PROCESSING FLOW**

202 **Data preprocessing**

203 We use data from 55 broadband seismic stations of EarthScope's USArray Transportable
204 Array (TA) recorded during July, 2012, within and around the northern Mississippi embayment
205 (Fig. 2) to demonstrate our ambient noise data processing flow. Velocity models for this area are
206 developed using full waveform tomography of the EGFs extracted from all temporary and
207 permanent stations. The crustal and upper mantle structures underneath the northern Mississippi
208 embayment are investigated. These models will be the subject of future reports.

Fig.2

209 In order to compare the robustness of our method, we compare cross-correlations and
210 dispersion curves with those computed based on time domain normalization (TDN). The
211 "MSNoise" package (Lecocq et al., 2014) is a python package which implements the TDN
212 method.

213 We first download daily vertical component waveform data for each station through the
214 IRIS (www.iris.edu) FDSN web service and work with them in SAC format, remove the

instrument response, remove the mean and trend, apply a bandpass filter from 0.02Hz to 1Hz and downsample the sampling rate from 40Hz to a 5Hz. The reason why we choose the passband 0.02-1Hz is that previous studies (e.g. Liang et al., 2008; Langston et al., 2009; Liu et al., 2018a; Yang & Langston, 2019) observed prominent surface wave arrivals in this frequency band. Downsamping the sampling rate to 5 Hz not only reduces the storage but also reduces the computation time of cross-correlations. Small events are usually higher frequency and are filtered out during the downsampling.

**CWT ambient noise data processing flow**

The temporal normalization step is replaced by the designaling method described above. After single station data preparation, the CWT designaling method is applied on each day of the data, followed by spectral whitening to provide spectrum-balanced data. A 5% taper is applied at the beginning and end of each data segment to avoid artifacts during cross-correlation. Each pair of stations are then cross-correlated and all one-day cross-correlograms for the month are stacked to increase the SNR.

In order to estimate the noise statistics for each day, we need to find a segment of the data that only contains noise. This is realized by a simple algorithm. For each day's data, we divide the time series into 48 half hour segments. The maximum absolute value in each segment is determined and the segment with the minimum absolute value is chosen to estimate noise statistics. There is no guarantee that earthquakes or other signals will not appear within the selected segment, but it provides a fast and accurate way to find this estimate. The time duration for each segment could be shorter when teleseismic events occur more frequently but each

segment still needs to be long enough to make a robust estimate. The test in Fig. 2 shows that the noise level could be estimated accurately with data time series as short as 500 seconds.

Besides removing the signal, soft thresholding can also be used to remove the noise in the final stacked EGFs to increase the SNR (equation 4). This step is applied to deliver the final EGFs.

Our new ambient noise data processing flow can be summarized into the following steps:

Step 1: Pre-processing: prepare waveform data for each station individually, which includes cutting the data into intervals of one-day, removing the instrument response, removing the mean and trend, applying a bandpass filter and resampling the data to a 5Hz sampling rate.

Step 2: Designal: for each one-day time series for a station, apply the soft thresholding designaling method to remove earthquakes and other transients.

Step 3: Spectral whitening, cross-correlation and stack: applying spectral whitening for each one-day time series for a station to provide a broader-band and spectrum-balanced data. Calculate the cross-correlation for each possible day and each station pair. Stack the desired number of day-correlations for each station.

Step 4: Applying the soft thresholding denoising method to remove the noise in each of the stacked cross-correlograms.

After step 4, we get the final EGFs for a pair of station, which can then be used to measure group and phase velocity (Liu et al., 2019) or to do full waveform tomography (Yang & Langston, 2019) to determine earth structure.

## RESULTS

We first apply the designaling algorithm to "synthetic" seismic data constructed from real data. The whole designaling procedure can be better examined and compared with the known noise input signal. Next, the entire flow will be applied to our subset of the TA array data and compared with results from using TDN.

In our implementation of the CWT, we use the Morlet wavelet as the mother wavelet $\psi(t)$ in equation (1) and (3) with 16 voices per octave. The designaling method is not sensitive to the number of the decomposition levels and smaller scale numbers will speed up the whole processing (Mousavi and Langston, 2016). Using 16 voices per octave in the processing is large enough for resolution while retaining efficiency. Choosing the right mother wavelet is also a difficult task. Different target problems require different optimal wavelets. We tried a number of different mother wavelets and by comparing the RMS error between the input noise and the final designaled results from the synthetic test, we achieve the least misfit using the Morlet wavelet. Therefore, we will use the Morlet wavelet in our data processing.

### Synthetic Data

To best simulate real data, we construct a synthetic time series by using two segments of recorded seismograms at station U41A. One segment contains 3,000 seconds of ambient noise data. The other seismogram segment is with the same length but contains a teleseismic event. The ambient noise segment is chosen to make sure that there is no earthquake or other obvious transient signal in the selected time period by looking at the seismogram in the time domain and the scalogram in the CWT domain. A teleseismic event occurred on July 25, 2012, was recorded by the station and is used as the earthquake input. The soft thresholding denoising algorithm is

first applied on the earthquake segment to remove any ambient noise contained in the seismogram. Then, both the ambient noise segment and the denoised earthquake segment are filtered with a 1Hz low-pass filter. The earthquake segment is then tapered before the first arrival time and at 1400 seconds to make sure there is no noise or signal before or after. The ambient noise segment and the teleseismic event segment are then summed to produce the final synthetic data (Fig. 3). Fig.3

The CWT spectrum of the synthetic data is calculated and shown in Fig. 3(d). The earthquake and ambient noise are clearly distinguished and are indicated in the spectrum. The CWT spectrum for ambient noise only falls into a specific range of scales and keeps a very stable amplitude pattern. These scales correspond to the main frequency band of the ambient noise. The earthquake contains signals over a wider range of scales which corresponding higher scale or lower frequency data and with much larger amplitude. The CWT spectrum for the earthquake is also changing with time and the pattern looks irregular. The overlapping scale band between the earthquake data and the ambient noise data makes it impossible to separate them by just using a bandpass filter.

After 1500 seconds, the seismogram is pure ambient noise and we use this segment to calculate the ECDF of the ambient noise and estimate the noise level for each scale. After obtaining the statistical properties of the ambient noise, we will decide whether the CWT spectrum is kept the same or modified by using the criteria in equation (10). The CWT spectrum after soft thresholding and the final designaled seismogram are shown in Figs 3e and f. The designaling algorithm removes most of the earthquake signal and the noise superficially looks the same before and after designaling. The time series after designaling looks more like the original ambient noise since it has a balanced amplitude throughout. A comparison of particular

306 time windows before and after designaling is also shown in Figs 3g and h. Noise is not modified
307 by this algorithm and appears qualitatively the same before and after designaling. The CWT
308 spectrum of the designaled time series is like a clipped version of the original spectrum which
309 suggests that there is still some small effects of the teleseism in the time series. We compare the
310 Fourier amplitude spectrum of input noise, input synthetic data and final designaled results (Fig.
311 4). The designaled time series has a slightly larger amplitude spectrum than the original spectrum
312 of the input noise due to the existence of some signals. But overall, the designaled result shows
313 very good amplitude recovery.

Fig. 4

314

315 **Real Data**

316 All of data recorded by the selected TA stations during July 2012 are used as input data
317 to test the new processing flow. We will use the station V44A (Fig. 2) which is located within
318 the NMSZ as an example to show the results. There are plenty of earthquakes and transient
319 signals appearing in the original recording (Fig. 5), which make it perfect to test the new
320 processing flow. For comparison, we also process the same data with TDN as a benchmark.

Fig. 5

321 Station V44A and S38A are used to show the details of each processing step (Fig. 6). A
322 teleseismic event is obviously present in these particular data. Ambient noise is barely seen and
323 is buried beneath the earthquake signals. Earthquake signals are efficiently removed after soft
324 threshold designaling and we get an amplitude-stable time series. Both stations show similar
325 results and no obvious earthquakes or transient signals are seen in the data after designaling.

Fig. 6

326 The designaled data are then correlated. The cross-correlogram from the soft thresholding
327 designaled data has higher SNR compared with the one from TDN. The Rayleigh wave at
328 positive time lags is not clearly seen in the result using TDN. The running absolute mean

329 normalization method will only balance the amplitude of the original data to match the amplitude
330 of the ambient noise. However, the spectrum is dominated by the truncation of peaks and troughs
331 of the high amplitude signal in the time domain that non-linearly increases its high frequency
332 parts. Truncating the CWT is less severe because individual wavelets are intrinsically smooth
333 and are smoothed yet again during the inverse transform integration. The data of the two
334 stations for other days are processed in the same way and the final one-month stacked cross-
335 correlogram calculated from our processing flow also shows higher SNR (Fig. 6d). The
336 designaling method removes earthquakes and other transient signals in a physical meaningful
337 way and it does not touch any ambient noise data. TDN achieves temporal normalization but
338 modifies the ambient noise while using a relatively harsh way to balance the amplitude of the
339 whole time series. We suggest that CWT designaling preserves more of the noise characteristics
340 within the event time window.

341 After correlation and stacking, random noise is still clearly seen in the stacked EGF. To
342 further increase the SNR, we apply soft threshold denoising on the stacked EGF (Fig. 6e). This
343 will remove much of the noise within the final stacked cross-correlogram and give us an even
344 higher SNR result.

345 A more dramatic example is shown in Fig. 7. One-month correlation results are stacked Fig. 7
346 for stations W42A and W46A to get the EGF. Fourier filtering and the soft threshold denoising
347 method are applied to improve the SNR of the stacked EGF. The noise frequency range overlaps
348 with the signal frequency range. After the low-pass filter, noise is still obvious in the EGF and
349 the SNR does not increase significantly. However, with the soft threshold denoising method, the
350 noise is removed and the denoised EGF has a very high SNR, which provides for better input in
351 later processing steps, such as group and phase velocity extraction.

Fig. 8 shows a record section of final EGFs for master station V44A from our processing flow and TDN. Both processing flows give clear EGFs. Symmetric Rayleigh waves are also observed. To better compare the two processing flows quantitatively, we compute the SNR by using the ratio of maximum amplitude between -200s and 200s and the maximum amplitude for the rest of data. Our new processing flow gives five to ten times higher SNR over using TDN. Rayleigh waves are clearly observed on both positive and negative time lags with smaller amplitude noise in between. Fig. 8

The next step after acquiring the final EGFs is to calculate phase or group velocities between each station pair. Althought this is not the primary purpose of this paper, it is useful to examine the differences in results obtained using the two data processing schemes. Readers may refer to other studies and reports (e.g. Yao et al., 2006; Bensen et al., 2007) for more details of dispersion calculation. Here, we show a comparison of the group velocities determined from EGFs between the two processing flows for one station pair (Fig. 9). We calculated the group velocity dispersion curve for station S38A using frequency-time analysis (Dziewonski et al., 1969). Although group velocities have significant overlap between the two methods, they clearly have different trends for periods greater than 15s. It is likely that these changes in the dispersion curves will give rise to differnces in the resulting velocity models. Fig. 9

## DISCUSSION

When deciding which processing flow to use for a specific dataset, we should observe how many earthquakes and other transient signals are contained in the data. In the interest of computational efficiency, if there are few transient events then CWT designaling may be overkill, wasting valuable compute cycles.

375 The new processing flow will deliver reliable and high SNR EGFs, which will be very
376 helpful in further processing steps, such as studying the attenuation or extracting body waves
377 from ambient noise seismic interferometry. However, some drawbacks of our processing flow
378 still need to be considered. The main concern is its relatively high computational cost. The CWT
379 is the most time-consuming part, which requires many forward and inverse Fourier transforms.
380 When processing large datasets such as years of ambient noise recording from large networks,
381 the computational time to designal will not be insignificant. Based on our processing experience,
382 it will take about half a minute to designal one-day of data for one station on a Macbook Pro
383 laptop. One possible solution is to use graphic processor unit (GPU) to calculate the wavelet
384 transform and remove the signals when processing large amounts of data, which will speed up
385 the processing significantly. It will take about 8 seconds to designal one-day of data for all 55
386 stations on a NVDIA V100 GPU. Another possibility is to check the data first and only apply the
387 soft threshold designaling if signals are observed in the data. In this study, we only processed
388 one-month of data at 55 stations and the time for the processing is acceptable.
389 Another assumption for this method is that the ambient noise time series should be stable
390 in that its statistical properties should not change significantly in each one-day data segment. If
391 such changes are observed in the data, the largest noise level should be used in the designaling
392 process to avoid accidentally removing any ambient noise.
393 Ambient noise tomography has been widely used during the last 15 years and will be
394 continuously developed in the future. Acquiring more reliable EGFs and getting more
395 information from seismic interferometry will make this method more powerful and robust.
396
397

## CONCLUSIONS

We propose a new ambient noise data processing flow to compute reliable EGFs. The denoising and designaling algorithm is based on the CWT with soft thresholding and is essential to this flow. The whole processing flow is automated without any manual interference. The new processing flow is suitable for data containing regional and teleseismic events or other transient signals. The whole processing flow is divided into four steps: (1) single station data preparation, (2) remove earthquakes and other transient signals in the seismic record, (3) spectrum whitening, cross-correlation and temporal stacking, (4) remove the noise in stacked cross-correlogram to deliver the final EGFs. The final EGFs can be used to extract phase or group velocity or to invert for velocity structure by full waveform tomography.

The principal step during data preparation is to acquire pure ambient noise that is free of earthquake and other transient signals (instrument irregularities and non-stationary noise sources near to stations, etc.). We adopt a method based on the CWT to remove these unwanted signals. The intrinsic time-frequency property of the CWT makes it possible to isolate noise and signal efficiently. A segment of pure ambient noise is usually obtainable and can be used to estimate the statistical property of the noise in the CWT domain. The estimated noise statistical properties are then used as a guide to detect whether the data point at different time and scales in the CWT domain is noise or not. A soft thresholding method is used to remove the signal if the data exceeds the noise level. We constructed synthetic data based on recorded noise and an earthquake to successfully test the method. Use on more extensive data shows excellent signal removal. Other denoising algorithms based on the CWT such as block thresholding (Mousavi et al., 2016) could also be used to remove earthquakes and other signals in the time series but they also require much more computational cost. Our method is efficient for large datasets.

The denoising method can also be used to remove the noise in the final EGFs to further increase the SNR. We use the same algorithm as in the designaling step but in a reverse manner to significantly increase the SNR in the final EGF. This denoising method performs better than bandpass filters since a Fourier filter has no time resolution.

We applied our processing flow to one-month of data from EarthScope TA stations near the NMSZ. Many earthquakes and other transient signals were recorded by the stations which make this dataset an appropriate test dataset for the algorithm. We obtain better EGFs with higher SNR than results using TDN. Except for removing earthquake and other transient signals that obscure the ambient noise data, and noise removal for the final stacked empirical Green's function, our processing flow is basically the same as previously proposed (Bensen et al., 2007). In regions where few earthquakes occur, there should not be many differences in the resulting EGFs between these two processing flows. However, the stacked EGF denoising step is recommended for both methods because it has relatively low computational cost but dramatically increases the SNR.

## DATA AND RESOURCES

Seismogram data used in this study are collected from IRIS (http://www.iris.edu, last accessed on January 2019). A MATLAB GUI code to process simple dataset and visualize the results from the CWT denoising and designaling method used in this study can be accessed at http://www.ceri.memphis.edu/people/clangstn/software.html (last accessed on August 2019). A CPU/GPU code to process large ambient noise datasets can be downloaded from https://github.com/SwiftHickory/bc_denoise.git (last accessed on August 2019).

## ACKNOWLEDGEMENT

We are grateful for financial support from the Center for Earthquake Research and Information to perform this research. This research was supported by the Air Force Research Laboratory under contract FA9453-18-C-0064.

## REFERENCE

Ansari, A., Noorzad, A., Zafarani, H. & Vahidifard, H., 2010. Correction of highly noisy strong motion records using a modified wavelet denoising method, Soil Dynam. Earthq. Eng., 30, 1168–1181.

Beenamol, M., Prabavathy, S. & Mohanalin J., 2012. Wavelet based seismic signal de-noising using Shannon and Tsallis entropy, Comput. Math. Appl., 64, 3580–3593.

Bensen, G. D., Ritzwoller, M. H., & Shapiro, N. M., 2008. Broadband ambient noise surface wave tomography across the United States, J. Geophys. Res., 113(B5).

Bensen, G. D., Ritzwoller, M. H., Barmin, M. P., Levshin, A. L., Lin, F., Moschetti, M. P., ... & Yang, Y., 2007. Processing seismic ambient noise data to obtain reliable broadband surface wave dispersion measurements, Geophys. J. Int., 169(3), 1239-1260.

Chik, Z., Islam, T., Rosyidi, S. A., Sanusi, H., Taha, M. R. & Mustafa, M. M., 2009. Comparing the performance of Fourier decomposition and wavelet decomposition for seismic signal analysis, Eur. J. Scientif. Res., 32, 314–328.

Cox, R. T.,Van Arsdale, R. B. & Harris, J. B., 2001. Identification of possible Quaternary deformation in the northeastern Mississippi Embayment using quantitative geomorphic analysis of drainage-basin asymmetry, Geol. Soc. Am. Bull., 113(5), 615-624.

466 Daubechies, I., 1992. Ten Lectures on Wavelets, Vol. 61, SIAM, Philadelphia, Pennsylvania,
467 357 pp., doi: 10.1137/1.9781611970104.

468 Dunn, M., DeShon, H. R., & Powell, C. A., 2013. Imaging the New Madrid seismic zone using
469 double-difference tomography, J. Geophys. Res., 118(10), 5404-5416.

470 Dziewonski, A.M., Bloch, S. & Landisman, M., 1969. A technique for the analysis of transient
471 seismic signals, Bull. Seism. Soc. Am., 59, 427– 444.

472 Elad, M., & Aharon, M., 2006. Image denoising via sparse and redundant representations over
473 learned dictionaries, IEEE Trans. Image Process., 15, 3736–3745.

474 Emry, E. L., Shen, Y., Nyblade, A. A., Flinders, A. & Bao, X., 2018. Upper Mantle Earth
475 Structure in Africa From Full-Wave Ambient Noise Tomography, Geochemistry,
476 Geophysics, Geosystems, 20(1), 120-147.

477 Farge, M., 1992. Wavelet transforms and their applications to turbulence, Annu. Rev. Fluid
478 Mech., 24, 395–458, doi: 10.1146/annurev.fl.24.010192.002143.

479 Gao, H., & Shen, Y., 2014. Upper mantle structure of the Cascades from full-wave ambient noise
480 tomography: Evidence for 3D mantle upwelling in the back-arc, Earth and Planetary
481 Science Letters, 390, 222-233.

482 Hildenbrand, T. G., 1985. Rift structure of the northern Mississippi embayment from the analysis
483 of gravity and magnetic data, J. Geophys. Res., 90(B14), 12607-12622.

484 Johnston, A. C., & Schweig E. S., 1996. The enigma of the New Madrid earthquakes of 1811-
485 1812, Anna. Rev. Earth Planet. Scie., 24, 339-384.

Langston, C. A., & Mousavi, S. M., 2019. Separating signal from noise and from other signal using non-linear thresholding and scale-time windowing of continuous wavelet transform, Bull. Seism. Soc. Am., accepted for publication.

Langston, C. A., Chiu, S. C. C., Lawrence, Z., Bodin, P., & Horton, S., 2009. Array observations of microseismic noise and the nature of H/V in the Mississippi embayment, Bulletin of the Seismological Society of America, 99(5), 2893-2911.

Lecocq, T., Caudron, C. & Brenguier, F., 2014. MSNoise, a python package for monitoring seismic velocity changes using ambient seismic noise, Seismological Research Letters, 85(3), 715-726.

Liang, C., & LangstonC. A, 2008. Ambient seismic noise tomography and structure of eastern North America. J. Geophys. Res., 113(B3).

Lin, F. C., Moschetti, M. P. & Ritzwoller, M. H., 2008. Surface wave tomography of the western United States from ambient seismic noise: Rayleigh and Love wave phase velocity maps, Geophys. J. Int., 173(1), 281-298.

Liu, C., Langston, C. A. & Powell C. A., 2019. Crustal and uppermost mantle shear wave velocity and radial anisotropy beneath the Missisippi embayment from ambient noise tomography, manuscript submitted for publication.

Mousavi, S. M. & Langston, C. A., 2016, Hybrid Seismic Denoising Using Higher-Order Statistics and Improved Wavelet Block Thresholding, Bull. Seismol. Soc. Am., 106(4), 1380-1393.

506 Mousavi, S. M., Langston, C. A. & Horton, S. P., 2016. Automatic micro-seismic denoising and
507 onset detection using the synchrosqueezed-con- tinuous wavelet transform, Geophysics,
508 81(4), 1–15, doi: 10.1190/ GEO2015-0598.1.

509 Nyamwandha, C. A., Powell, C. A. & Langston, C. A., 2016. A joint local and teleseismic
510 tomography study of the Mississippi Embayment and New Madrid Seismic Zone, J.
511 Geophys. Res. B Solid Earth Planets, 121(5), 3570-3585.

512 Pazos, A., Gonzalez, M. J. & Alguacil, G., 2003. Non-linear filter using the wavelet transform
513 applied to seismological records, J. Seismol., 7, 413–429.

514 Powell, C. A., Withers, M. M., DeShon, H. R. & Dunn, M. M., 2010. Intrusions and anomalous
515 Vp/Vs ratios associated with the New Madrid seismic zone, J. Geophys. Res. B Solid
516 Earth Planets, 115(B8).

517 Rioul, O. & Duhamel, P., 1992. Fast algorithms for discrete and continuous wavelet
518 transforms, IEEE transactions on information theory, 38(2), 569-586.

519 Sabra, K. G., Gerstoft, P., Roux, P., Kuperman, W. A. & Fehler, M. C., 2005. Extracting time-
520 domain Green's function estimates from ambient seismic noise, Geophysical Research
521 Letters, 32(3).

522 Shapiro, N. M., Campillo, M., Stehly, L. & Ritzwoller, M. H., 2005. High-resolution surface-
523 wave tomography from ambient seismic noise, Science, 307(5715), 1615-1618.

524 Starck, J. L., Murtagh, F. & Fadili, J. M., 2010. Sparse Image and Signal Processing. New York:
525 Cambridge University Press.

526 Tary, J. B., Herrea, R. H., Han, J. & Baan, M. V. D., 2014. Spectral estimation—What is new?
527 What is next? Rev. Geophys., 52(4), 723–749, doi: 10.1002/2014RG000461.

528 Thomas, W. A., 2006, Tectonic inheritance at a continental margin, GSA today, 16(2), 4-11.

529 To, C. A., Moore, J. R. & Glaser, S. D., 2009. Wavelet denoising techniques with applications to
530 experimental geophysical data, Signal Process., 89, 144–160, doi:
531 10.1016/j.sigpro.2008.07.023.

532 Torrence, C. & Compo, G. P., 1998. "A practical guide to wavelet analysis." Bulletin of the
533 American Meteorological Society, 79(1), 61-78.

534 Tuttle, M. P., Schweig, E. S., Sims, J. D., Lafferty, R. H., Wolf, L. W. & Haynes, M. L., 2002.
535 The earthquake potential of the New Madrid seismic zone, Bull. Seismol. Soc. Am.,
536 92(6), 2080-2089.

537 Van Arsdale, R. & Cupples, W., 2013. Late Pliocene and Quaternary deformation of the Reelfoot
538 rift, Geosphere, 9(6), 1819-1831.

539 Van Arsdale, R., Bresnahan, R., McCallister, N. & Waldron, B., 2007. Upland Complex of the
540 central Mississippi River valley: Its origin, denudation, and possible role in reactivation
541 of the New Madrid seismic zone, Geological Society of America Special Papers, 425,
542 177-192.

543 Wapenaar, K. & Fokkema, J., 2006. Green's function representations for seismic
544 interferometry, Geophysics, 71(4), SI33-SI46.

545 Weaver, J. B., Yansun, X., Healy, D. M. & Cromwell, L. D., 1991. Filtering noise from images
546 with wavelet transforms, Matnetic Resonance in Medicine, 21, 288-295.

547 Yang, Y. & Langston, C. A., 2019. Full waveform ambient noise tomography for the northern
548 Mississippi embayment, unpublished manuscript.

549 Yao, H., van Der Hilst, R. D. & De Hoop, M. V., 2006. Surface-wave array tomography in SE
550 Tibet from ambient seismic noise and two-station analysis—I. Phase velocity
551 maps, Geophys. J. Int., 166(2), 732-744.

552 **FIGURES**

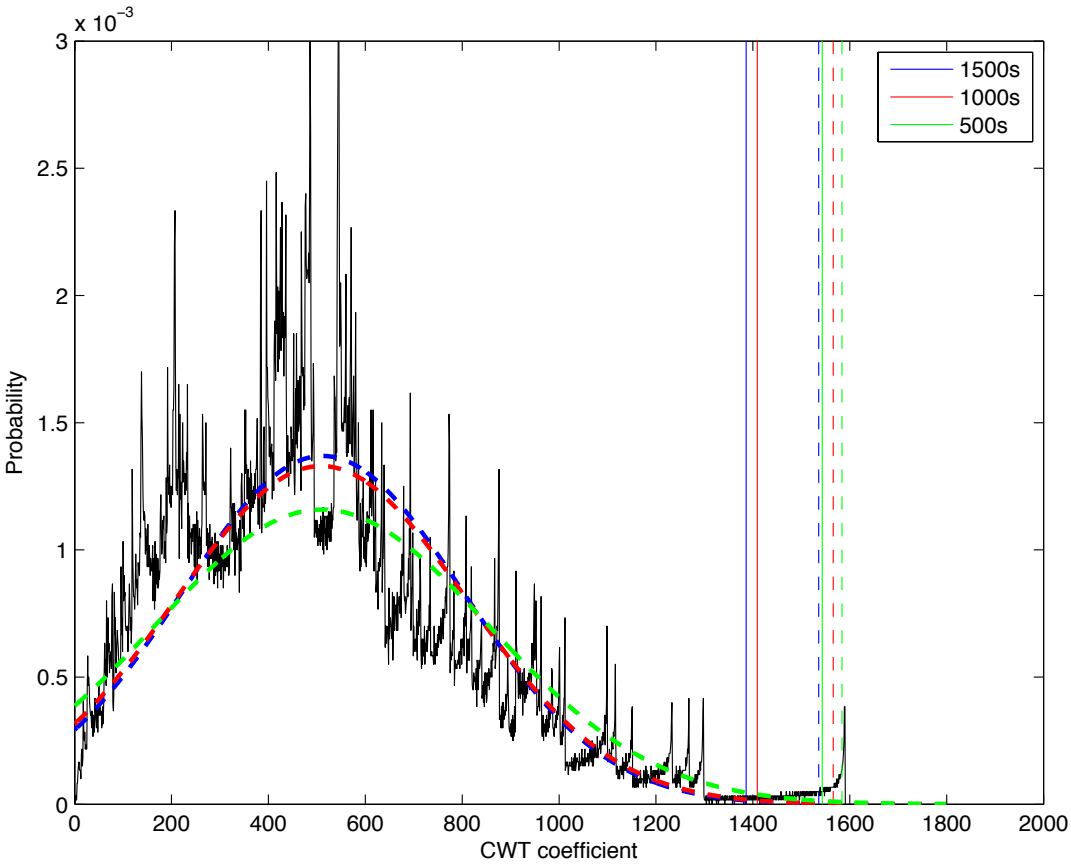


553

554 Figure 1. Empirical probability density function of the ambient noise CWT coefficients (black
555 line) and the estimated probability density function (dashed line) with the assumption of normal
556 distribution. The ambient noise data used for this plot are shown in the synthetic test figure. The
557 empirical probability density function is plotted only with 1500s data and the noise level is
558 estimated with different data length of 1500s, 1000s and 500s, respectively. The vertical solid
559 line and dashed line show the estimated noise level based on Gaussian distribution and empirical
560 probability distribution with 99% confidence value, respectively. Notice that the estimated noise
561 level is more stable with ECDF method.

562

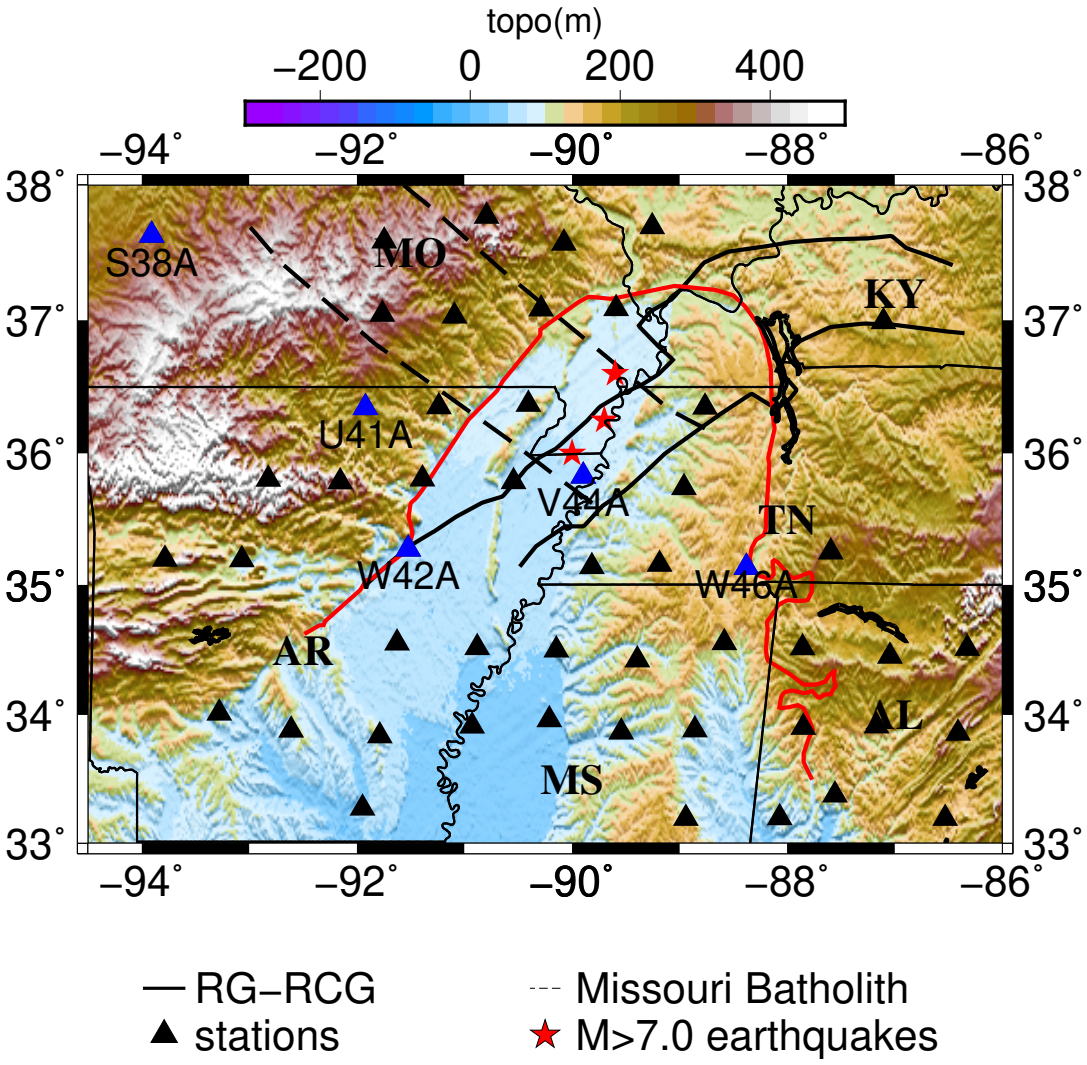


Figure 2. The distribution of the seismic stations used in this study (filled triangles). Continuously seismic recordings during July 2012 from a subset of the USArray Transportable Array stations in and around the northern Mississippi embayment are our benchmark test dataset. Major geological features include the Reelfoot Graben (RG), Rough Creek Graben (RCG) and Missouri batholith (between two dashed lines). The boundary of the Mississippi embayment is shown by the red lines. The locations of the three large earthquakes that occurred in 1811 and 1812 are shown as the red stars (Johnston & Schwieg, 1996). Several specific stations used as examples in the rest of this article are annotated.

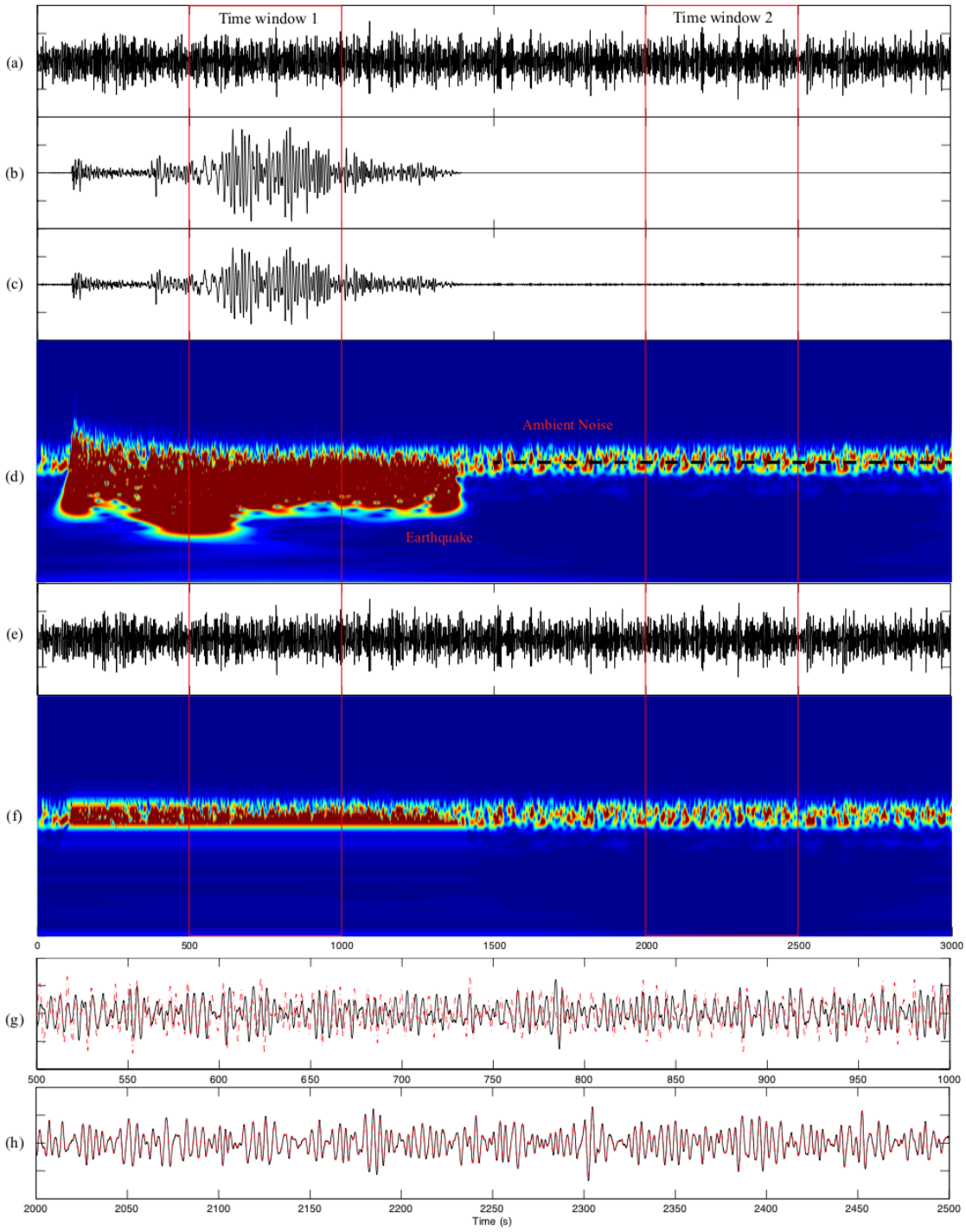


Figure 3. Designaling synthetic test based on recorded ambient noise and earthquake data. (a) 3000s ambient noise data from station U41A. (b) The July 25, 2012, teleseismic earthquake recorded by station U41A. The data are denoised with the CWT soft thresholding denoising

577 algorithm and a 1Hz low-pass filter is applied after denoising. Data before the first arrival and
578 after 1400 seconds are tapered. (c) Synthetic data constructed by summing ambient noise data in
579 (a) and seismic event data in (b). (d) The modulus of the complex CWT spectrum of synthetic
580 data in (c). The dashed line indicates the data used in (a). (e) Synthetic data after designaling
581 shown in the time domain. (f) Synthetic data after designaling shown in the CWT domain. (g)
582 The comparison of seismic data before designaling (solid line) and after designaling (dashed
583 line) with the data in the time window 1. (h) Same as (g) but for time the window 2. The vertical
584 red lines delineate the two 500s time windows.

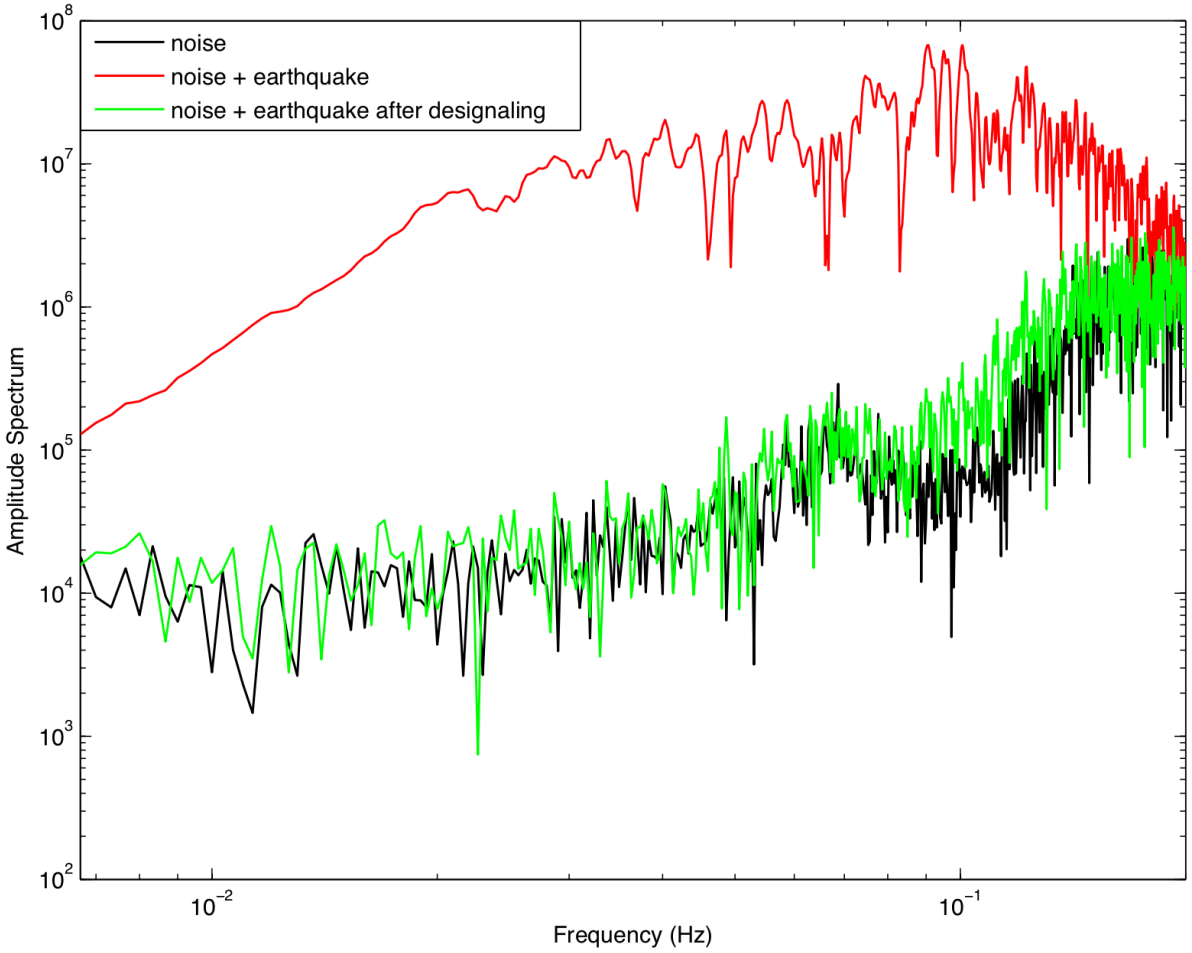


585

586 Figure 4. The comparison of the Fourier amplitude spectrum between the original noise data, the

587 noise data added with earthquake data and the final designaled data.

588

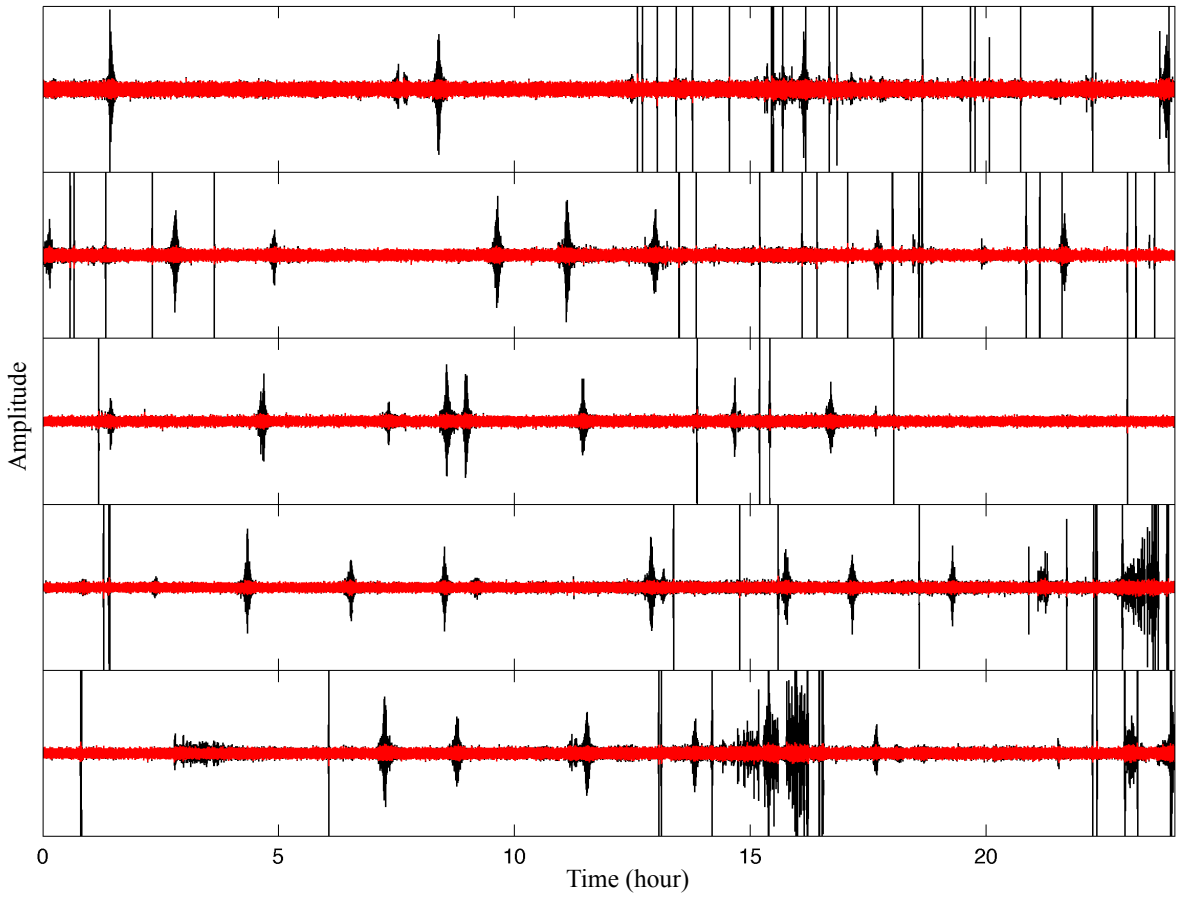


589

590 Figure 5. Vertical component seismograms of station V44A recorded during the first five-days of
591 July 2012 (black) and the designaled result (red). Each row shows one-day of seismic data. There
592 are many earthquakes and transient signals recorded by the station. These signals are
593 successfully removed after designaling.

594

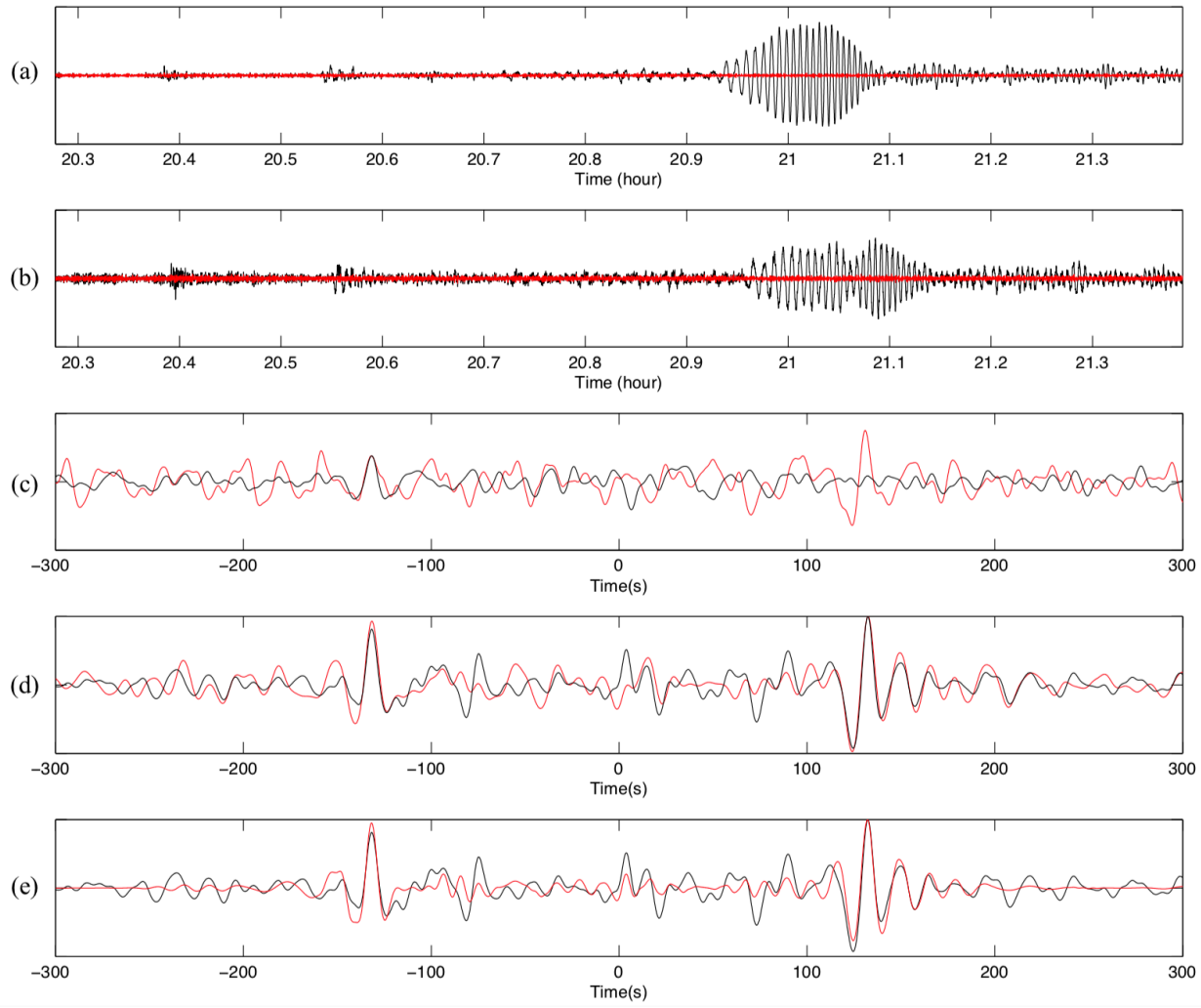


Figure 6. EGF calculation between station V44A and S38A. (a) A segment of seismic record for station S38A on July 28, 2012, with the black line indicating the original data and the red line showing the designaled results. A teleseismic event is seen within this time period and is removed after designaling. (b) Same as (a) but for station V44A. (c) One-day cross-correlation between station S38A and station V44A for date July 28, 2012, calculated using TDN (black) and the designaled data (red). (d) One-month stacked cross-correlogram obtained from TDN (black) and our processing flow before the final denoising step (red). (e) One-month stacked cross-correlogram obtained from TDN and our processing after the final denoising step (red). Absolute amplitude is plotted in (c). The amplitude is normalized in (d) and (e).

605

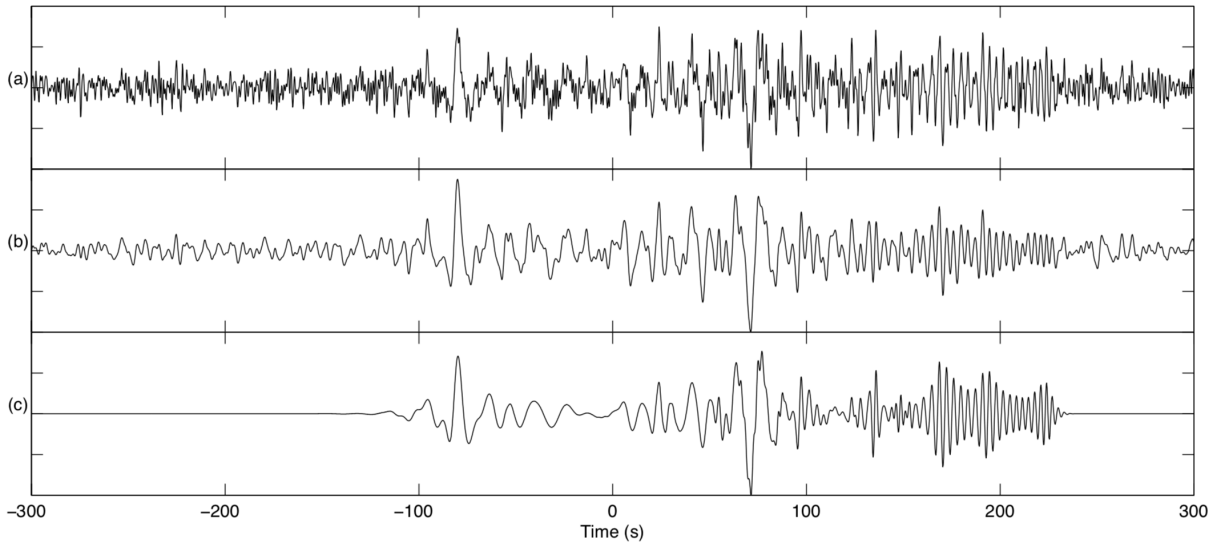


606

607 Figure 7. Application of soft threshold denoising on the final stacked cross-correlogram for
608 stations W42A and W46A. (a) Original stacked cross-correlogram. (b) Stacked cross-
609 correlogram with a 0.3Hz low-pass filtered applied. (c) Stacked cross-correlogram after soft
610 thresholding denoising.

611

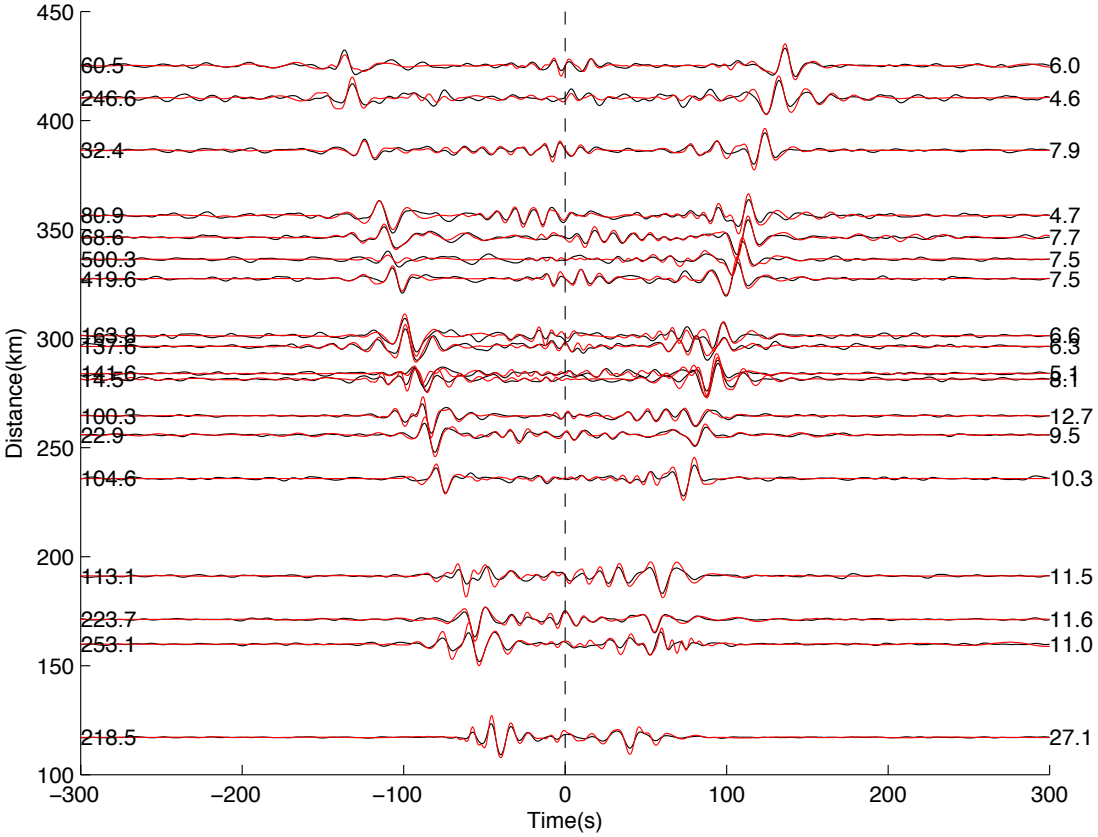


612

613 Figure 8. EGFs record section acquired from TDN (black) and our processing flow (red) for
614 station V44A. SNR for the results from TDN is shown on the right side and for our method on
615 the left side. The SNR is calculated using the ratio between the maximum amplitude from the
616 time window -200s to 200s and maximum amplitude of the remaining part. A bandpass filter
617 between 0.01s and 0.15s is applied to all data. The amplitude is the stacked absolute amplitude
618 without normalization.

619

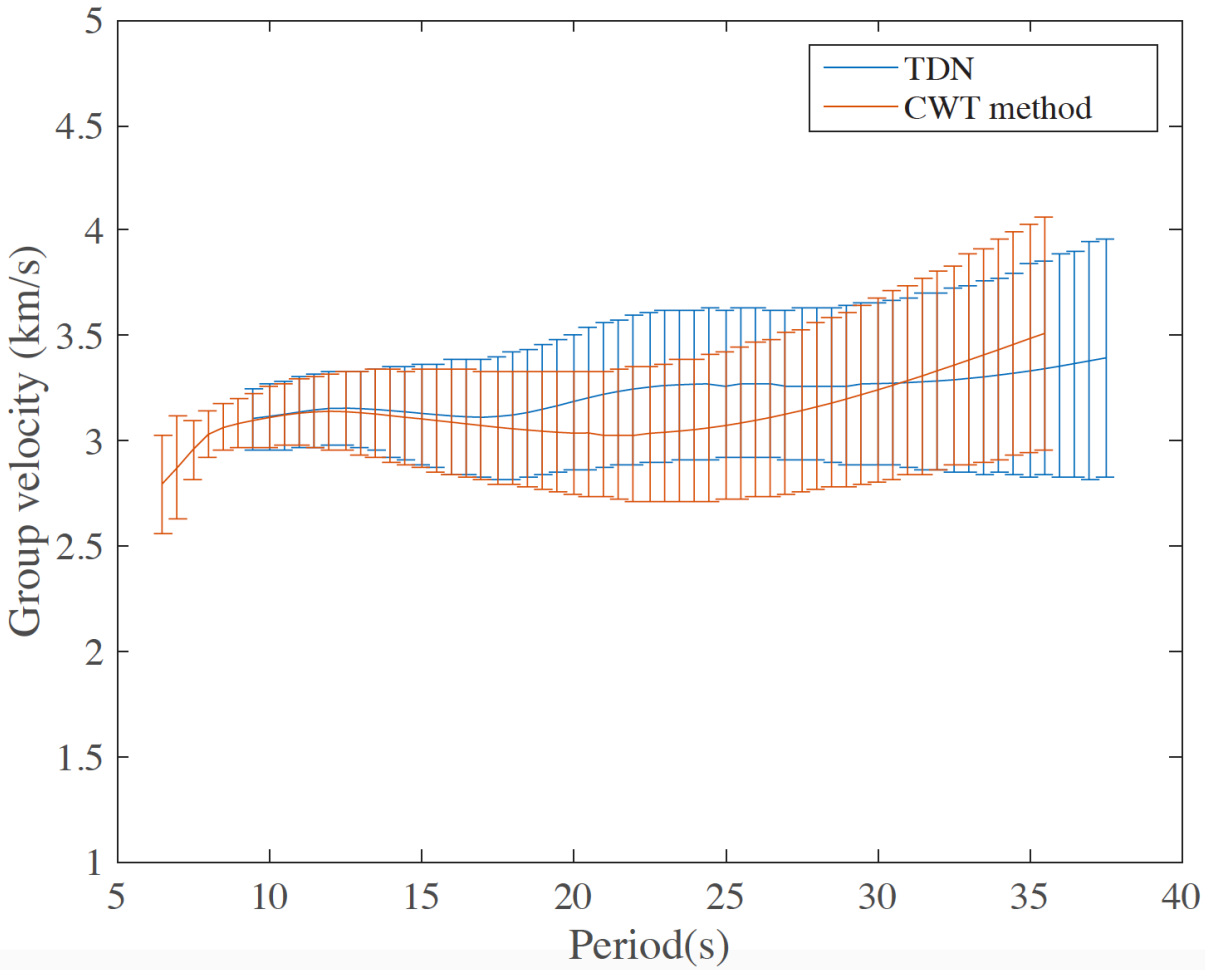


620

621 Figure 9. Comparison of group velocity dispersion curves from station V44A to station S38A

622 from an EGF using TDN (blue) and our processing flow (red).

623